Am J Cancer Res 2023;13(11):5610-5625
www.ajcr.us /ISSN:2156-6976/ajcr0151019

Original Article

CircATP13A1 (hsa_circ_0000919) promotes cell proliferation and metastasis and inhibits cell apoptosis in pancreatic ductal adenocarcinoma via the *miR-186/miR-326/HMGA2* axis: implications for novel therapeutic targets

Xiongzhi Wangpu[1], Jingkun Zhao[2], Chaoran Yu[3], Song Yu[1], Hongcheng Wang[1], Zhou Yuan[1], Xinyu Huang[1]

[1]Department of Hepatobiliary and Pancreatic Surgery, Shanghai 6th People's Hospital Affiliated to Shanghai Jiao Tong University, School of Medicine, No. 600 Yishan Rd, Shanghai 200233, China; [2]Department of Gastrointestinal Surgery and Minimally Invasive Surgery, Ruijin Hospital, Shanghai Jiao Tong University, School of Medicine, Shanghai 200001, China; [3]Department of General Surgery, Shanghai 9th People's Hospital, Shanghai Jiao Tong University, School of Medicine, Shanghai 200011, China

Received May 2, 2023; Accepted August 27, 2023; Epub November 15, 2023; Published November 30, 2023

Abstract: Pancreatic ductal adenocarcinoma (PDAC) is a notoriously aggressive malignancy with a survival rate of merely 9%. The prognosis in patients with PDAC is relatively poor, particularly in patients with advanced distant metastases. However, the mechanisms of PDAC progression remain elusive. Circular RNAs (circRNAs) have been implicated in the development of various malignancies, including PDAC. Therefore, this study aimed to investigate how a novel circRNA, *circATP13A1*, regulates PDAC progression. We used the GEO database to determine *circATP13A1* expression levels in cancer and adjacent cells and employed the limma package of R software to identify differentially expressed circRNAs. We detected the expression of *circATP13A1*, *miR-186*, and *miR-326* using qRT-PCR and investigated the effect of *circATP13A1* on cell proliferation, migration, invasion, and apoptosis *in vitro* using the Cell Counting Kit-8 (CCK-8), the transwell migration assay, and the flow cytometry assay. We then performed RNA pull-down assay, RNA immunoprecipitation (RIP), and Western blot to verify the interaction between *circATP13A1*, *miR-186*, *miR-326*, and *HMGA2*. Moreover, we used a naked mice model to determine how *circATP13A1* affects tumor growth and progression *in vivo*. Loss and gain of function analyses revealed that *circATP13A1* upregulation promotes cell proliferation, migration, invasion and tumor growth both *in vitro* and *in vivo*, which results in PDAC progression and poor prognosis in patients. *CircATP13A1* knockdown significantly impaired cell proliferation and migration of PDAC cell lines. Additionally, *circATP13A1* knockdown significantly increased the expression of *miR-186* and *miR-326*, while reducing the expression of *HMGA2* ($P < 0.05$), indicating that *miR-186* and *miR-326* are downstream targets of *circATP13A1*. Rescue experiments support the interactions between *circATP13A1*, *miR-186*, *miR-326*, and *HMGA2*. In conclusion, we demonstrated that *circATP13A1* sponges the *miR-186/miR-326/HMGA2/* axis, acting as an oncogene to promote PDAC development.

Keywords: *CircATP13A1*, PDAC, *miR-186*, *miR-326*, *HMGA2*

Introduction

Pancreatic cancer is a significant public health problem and ranks the seventh leading cause of cancer-related death worldwide [1]. It has a high mortality rate with around 200,000 deaths annually and will become the second leading cause of cancer-related death by 2030 [2, 3]. Pancreatic ductal adenocarcinoma (PDAC) arises from the epithelium lining of pancreatic ducts, accounting for over 90% of pancreatic cancer diagnoses, and the patients with PDAC have a low survival rate of about 9% [4-6]. Despite recent advances in the prevention, diagnosis, and treatment of PDAC, effective biomarkers and improved treatments are still lacking.

Circular RNAs (circRNAs) have been implicated in a variety of human diseases, including pan-

creatic cancer [7]. They function as gene expression regulators at the transcriptional level by interacting with RNA-binding proteins and have been used as diagnostic and prognostic biomarkers [8]. Up to now, over 20 circRNAs have been associated with pancreatic cancer. Among them, circ_0005105 [9], hsa_circ_0007367 [10], and circ_MTHFD1L [11] promote PDAC progression by sponging miRNAs to promote cell proliferation in cancer tissues [12].

MicroRNAs (miRNAs) are short, non-coding RNAs with approximately 17-25 nucleotides in length. MiRNAs contain a seed sequence through which they bind to the 3' untranslated region (3' UTR) of target mRNAs by complimentary matching, leading to mRNA degradation or translation inhibition [13, 14]. MiRNAs regulate cell development, differentiation, and apoptosis by simultaneously targeting several mRNAs, and they have been implicated in carcinogenesis, invasion, metastasis, and chemoresistance of cancer cells [15, 16]. For instance, downregulation of *miR-186* is closely related to the progression of acute myeloid leukemia (AML), multiple myeloma (MM), and glioma [17-19]. In contrast, upregulation of *miR-186* expression in PDAC and bladder cancer promotes cell proliferation, resulting in poor survival of cancer patients. In addition, *miR-326* plays various roles in cancer development and its overexpression can inhibit the progression of non-small cell lung cancer (NSCLC) [20, 21]. Reportedly, miRNAs can target several cancer-related genes to regulate cancer development [22].

High mobility group protein 2 (HMGA2) functions as a gene expression regulator by interacting with DNA regions with high AT content. Despite the roles in human body development, HMGA2 is involved in almost all known human malignancies [23]. In human colorectal cancer, *HMGA2* was downregulated by miR-330 [24], and it can inhibit tumor growth, metastasis, and angiogenesis that are initiated by p-53 [25]. However, how *HMGA2* interacts with novel *circATP13A1*, *miR-186*, and *miR-326* in PDAC remains unexplored.

Therefore, we aim to investigate the functional role of *circATP13A1* in regulating cell proliferation and migration as well as cancer progression in PDAC. The findings provide new insights into the function of *circATP13A1* in PDAC and unveil its clinical implications and potential as a biomarker and therapeutic target for PDAC.

Materials and methods

Tissue sample collection

Seventy-pair of surgical specimens including PDAC tissues and the neighboring normal pancreatic duct tissues were obtained from PDAC patients at Shanghai Sixth People's Hospital Affiliated with Shanghai Jiao Tong University, School of Medicine. The criteria for enrolling patients in the present study are: 1) confirmed PDAC by pathological examination; 2) surgical resection as primary treatment; 3) eligibility for surgery to collect fresh-frozen tumor and paired control tissues; 4) availability of main clinical data for study analysis. The patients were excluded if they: 1) received neoadjuvant therapy prior to surgery; 2) exhibited complications due to other malignant tumors; 3) acquired immune deficiency syndrome; 4) missed follow-up records [26]. All patients were informed of the significance of this study before the sample collection, and written informed consent was received from each patient. The samples were stored at -80°C prior to use. The study was approved by the Ethics Committee of Shanghai Sixth People's Hospital Affiliated with Shanghai Jiao Tong University, School of Medicine.

Cell lines and culture

The normal human pancreatic duct epithelial cell line (HPDE6c7) and PDAC cancer cell lines including AsPC-1, CFPAC, SW1990, BxPC-3, and Panc-1 were obtained from the American Type Culture Collection (ATCC) and cultured in DMEM (Thermo Fisher Scientific, Inc.) supplemented with 10% FBS, 100 U/ml penicillin, and 100 g/ml streptomycin (Beyotime Institute of Biotechnology) at 37°C.

Bioinformatics analysis

To determine *circATP13A1* expression in PDAC and normal adjacent cells, the GEO (Gene Expression Omnibus) database chip data were screened. The limma R software package (version 3.4.2) was used to visualize the heat map reporting the differentially expressed circRNAs between cancer and normal surrounding tissues.

Table 1. The list of primers for qPCR

Gene	Forward 5'-3'	Reverse 5'-3'
CircATP13A1	5'-GCACCTGAGGGACATTCTTTG-3'	5'-CGGGACACAGCCAGATTAGA-3'
miR-186	5'-TTAATTCCGATAACGAACGAGA-3'	5'-CGCTGAGCCAGTCAGTGTAG-3'
miR-326	5'-CTCTGGGCCCTTCCTC-3'	5'-GAACATGTCTGCGTATCTC-3'
U6	5'-CGCTTCCAGCACATATAC-3'	5'-CGCTTCGGCAGCACATATAC-3'
HMGA2	5'-GAGCCCTCTCCTAAGAGACCC-3'	5'-TTGGCCGTTTTTCTCCAATGG-3'
GAPDH	5'-GGAGCGAGATCCCTCCAAAAT-3'	5'-GGCTGTTGTCATACTTCTCATGG-3'

Target gene prediction

The circRNA interactome (https://circinteractome.nia.nih.gov/), TargetScan (http://www.targetscan.org/), and miRanda (http://www.microrna.org/) were used to predict the target miRNAs (*miR-186/miR-326*) for *circATP13A1*.

RNA isolation and quantitative polymerase chain reaction analysis

Total RNA was extracted from cells using TRIzol reagent (Thermo Fisher Scientific, Inc.) following the manufacturer's instructions. DNase I treatment and Phenol-chloroform purification were performed to remove genomic DNA contamination from RNA. Quantitative real-time polymerase chain reaction (qRT-PCR) was performed using the GeneAmp RNA PCR Kit (Applied Biosystems, USA) and the SYBR Green Quantitative PCR Master Mix. Real-time qPCR reactions were conducted with an initial denaturation at 95°C for 10 min, followed by 40 cycles of 15 s at 95°C and 1 min at 60°C for amplification. The expression levels of *circATP13A1* and *HMGA2* levels were normalized to that of *GAPDH*, while the expression levels of *miR-186* and *miR-326* were normalized to that of *U6*. Target gene expression was calculated using the $2^{-\Delta\Delta CT}$ method [27]. Primers for qRT-PCR were listed in **Table 1**.

RNase R treatment

To check the circular structure of *circATP13A1*, SW1990 and BxPC-3 pancreatic cell lines were incubated with actinomycin D (2 mg/ml). Then qRT-PCR was performed to assess the levels of *circATP13A1* and *ATP13A1* mRNA. Moreover, 10 mg of RNA samples were treated with RNase R and incubated at 37°C for 30 minutes, followed by qRT-PCR assessment of *circATP13A1* and *ATP13A1* mRNA.

Colony formation assay

PDAC cells were suspended in DMEM containing 10% FBS and seeded into a 6-well plate (1×10^4 cells/well) followed by incubation for two weeks at 37°C. The cells were then fixed in 4% paraformaldehyde for 15 min and stained with Giemsa (Beyotime, China) for 30 min. The stained cells were washed with PBS, air-dried, and counted with a light microscope.

Cell transfection

The full-length of *circATP13A1b* was cloned into the pLCDH-ciR vector (GenePharma, China). Small interfering RNA (siRNA) and the relevant control siRNA were synthesized by RiboBio (Guangzhou, China). The sequence of si-circATP13A1 was 5'-AGGGAGGTGAGGGCCTGGTGT-3'. The mimics, inhibitor, and corresponding negative controls (NCs) for *miR-186* and *miR-326*p were synthesized by GenePharma (Shanghai, China). The siRNAs, miRNA mimics, and miRNA inhibitor were transiently transfected into cells using Lipofectamine 3000 (Invitrogen, CA, USA) following the manufacturer's instructions.

Western blot

The cells were lysed with radioimmunoprecipitation (RIPA) buffer (Roche Diagnostics, Germany) and quantified using a BCA Protein Quantification Kit (Bio-Rad, USA) according to the manufacturer's instructions. The proteins were then separated by 10% SDS-polyacrylamide gel electrophoresis (PAGE) followed by transblotting to a polyvinylidene fluoride (PVF) membrane (Millipore, USA). Then, primary antibodies, including HMGA2 (ab246513, 1:2000) and GAPDH (ab9485, 1:2000) at 4°C for 8 hours were incubated with the PVF membrane followed by incubation with horseradish peroxidase-labeled anti-rabbit secondary antibodies

IgG H&L (HRP) (ab97051, 1:10000) at room temperature for 1 hour. Finally, a chemiluminescence detection kit (Beyotime, China) was used to determine protein expression.

Cell viability assay

Cell Counting Kit-8 (CCK-8, Dojindo Molecular Technologies, China) was employed to examine cell viability. After transfection, 2×10^5 SW1990 and BxPC-3 cells were seeded in 96-well plates and cultured in CO_2 (5%) with 10 μL of L-CCK-8 solution added at 0, 24, and 72 hours. Further, the cells were cultured at 37°C for an additional 4 hours. Finally, the optical density at 450 nm was measured using a microplate reader (BioRad, USA).

Luciferase reporter gene assay

The Dual-Luciferase Reporter Assay System psiCHECK (Thermo Fisher Scientific, Inc.) was used to perform the luciferase reporter gene assay. The luciferin reporter gene was cloned into wild-type (WT) and mutants of *circATP13A1*, *miR-186*, *miR-326*, and *HMGA2*. SW1990 and BxPC-3 cells (2×10^4 cells per well) were seeded in 24-well plates and cultured overnight. The cells were then transfected with WT or mutant reporter and *miR-186*p and *miR-326* mimics (10 nM) or mimics control (10 nM) using Lipofectamine® 3000 (Thermo Fisher Scientific, Inc.). After 48 hours, luciferase activities were measured using a Dual-Luciferase Detection Kit (Promega, USA). Renilla luciferase activity was used as the control.

RNA immunoprecipitation (RIP)

SW1990 and BxPC-3 cells were lysed with ice-cold lysis buffer, and the cell lysate was collected and incubated with magnetic beads pre-conjugated with immunoglobulin G (1:500) antibody or Argonaute2 (Ago2; 1:500). The co-immunoprecipitated RNAs were digested by proteinase K before total RNA isolation. Gene enrichment was assessed by qRT-PCR.

Transwell migration and matrigel invasion assays

Transwell plates with 8 μm pores (Millipore, USA) were used for the invasion and migration assays. Approximately 2×10^5 cells were digested and cultured in 200 mL serum-free medium in the upper chamber, and 600 μL medium was added to the lower chamber for the migration assay. For the invasion assay, Matrigel was used according to the manufacturer's protocols (BD Biosciences, USA). After 24 hours of incubation at 37°C, the cells in the lower chamber were fixed in 4% paraformaldehyde and stained with 0.1% crystal violet solution at room temperature for 10 min (Sigma-Aldrich; Merck KGaA). The invaded and migrated cells were quantified and counted in three different fields under an inverted light microscope (Zeiss, Primovert).

Nucleic acid electrophoresis

The amplicon of *circATP13A1* and linear *ATP13A1* from cDNA and genomic DNA were separated on a 2% agarose gel by electrophoresis for 45 min at 130 V using tris-acetic EDTA (TAE). Super DNA Marker (CWBIO, China) was used as a DNA marker, and the bands were visualized using ultraviolet radiation.

RNA-pull down assay

The RNA-pull down assay was employed to confirm the relationship between *circATP13A1* and *miR-186* and *miR-326*. The *circATP13A1* sequence and the control probes were synthesized by Sangon Biotech (Shanghai). Probe-coated beads were generated by co-incubation with streptavidin-coated beads for 2 hours at 25°C (Thermo Fisher Scientific, Inc.). SW1990 and BxPC-3 cells were collected, lysed, and incubated with *circATP13A1* probes overnight at 4°C. Next, the beads were eluted and the complex was purified with TRIzol® reagent (Takara Biotechnology Co., Ltd.). QRT-PCR was used to determine the levels of *miR-186*, *miR-326*, and *HMGA2*.

In vivo studies

Four-week-old nude mice were purchased from the animal center of Shanghai Sixth People's Hospital Affiliated with Shanghai Jiao Tong University, School of Medicine, and the animal experiment was approved by the ethics committee of Shanghai Sixth People's Hospital Affiliated with Shanghai Jiao Tong University, School of Medicine. Five mice per group were used to construct subcutaneous tumor formation models, and stable cell lines transfected

with *circATP13A1* and NC (0.1 ml of cell suspension vs 1 × 10^6 stable cells) were injected into the forelimb's axilla of the nude mice. The tumor volume was calculated using the formula (width^2 × length)/2 in 35 days.

Statistical analysis

GraphPad Prism version 7 and RStudio (version 4.0) were used for statistical analysis. Quantitative data were presented as mean ± SD. Unpaired student's *t*-test was used to measure the differences between two groups, and one-way ANOVA was used to compare multiple groups. Survival distributions and overall survival rates were analyzed using the Kaplan-Meier method. The significance between survival rates was determined by the rank test. Values of $P < 0.05$ were considered statistically significant.

Result

CircATP13A1 is highly expressed in PDAC tissues and cell lines

We obtained the circRNA expression profile from the GEO database and used the Limma R package to detect differentially expressed genes between PDAC and control tissues. In total, we detected 111 upregulated circRNAs and 57 downregulated circRNAs. Among the upregulated ones, *circATP13A1* was among the top 20 (|log2FC| $P < 0.05$; **Figure 1A**, **1B**). **Figure 1C** illustrates that *circATP13A1* is formed by the reverse splicing of exons 1-9 of the pre-mRNA located on CHR19: 19760861-1976115 (**Figure 1C**). To further investigate the differential expression of *circATP13A1* in tumor and normal tissues, we performed a qRT-PCR analysis on cancer and adjacent normal tissues from 70 PDAC patients. The results revealed that *circATP13A1* was significantly upregulated in PDAC tumor tissues compared to the adjacent normal tissues ($P < 0.05$, **Figure 1D**). Moreover, we divided the 70 PDAC patients into high and low expression groups based on the median expression value of *circATP13A1*. Then we used the KM-plotter curve to determine the overall survival of the two groups. We detected that the survival of the high *circATP13A1* expression group was generally poor compared to the low expression group ($P < 0.05$, **Figure 1E**). Moreover, we assessed *circATP13A1* expression in different pancreatic cancer cell lines. Results showed that *circATP13A1* expression was significantly higher in AsPC-1, CFPAC-1, BxPC-3, SW1990, and Panc-1 pancreatic cancer cell lines compared to HPDE6c7 cells. Because SW1990 and BxPC-3 cells exhibited the highest and lowest *circATP13A1* expression levels, respectively ($P < 0.01$, **Figure 1F**), they were selected for subsequent molecular experiments. Next, we used divergent and convergent primers to amplify *circATP13A1* and *ATP13A1* in SW1990 pancreatic cell line. The divergent primer could amplify the *circATP13A1* fragment (**Figure 1G**). We also investigated the resistance of *circATP13A1* to RNase. We extracted the total RNA including linear and *circATP13A1* from SW1990 pancreatic cancer cells, and treated them with mock (control) and RNase R for 30 minutes at 37°C. qRT-PCR revealed that *circATP13A1* was not degraded by RNase R compared to the control, while *ATP13A1* was readily digested by RNase R ($P < 0.01$, **Figure 1H**). Finally, we investigated the effect of actinomycin D on the expression of linear *ATP13A1* and *circATP13A1* in SW1990 cells. We observed that actinomycin D significantly reduced linear *ATP13A1* expression in a time-dependent manner, while *circATP13A1* expression remained unchanged ($P < 0.01$, **Figure 1I**).

CircATP13A1 promotes cell proliferation and metastasis as well as inhibits cell apoptosis in PDAC cells

To investigate the role of *circATP13A1*, we designed two small interfering RNAs against *circATP13A1* (si-circ*ATP13A1*#1/si-circ*ATP13A1*#2) and an overexpressed circRNA construct (oe-*circATP13A1*). The two siRNAs were then transfected into the SW1990 cell line, and the oe-*circATP13A1* construct was transfected into the BXPC3 cell line. QRT-PCR showed that both siRNAs significantly reduced *circATP13A1* expression in the SW1990 cell line compared to the control (si-NC). oe-*circATP13A1* significantly increased *circATP13A1* levels in the BXPC3 cell line ($P < 0.01$; **Figure 2A**).

We then evaluated the effect of *circATP13A1* on cell viability. The result indicated that *circATP13A1* knockdown significantly reduced the cell viability in the SW1990 cell line compared to si-NC. Conversely, the cell viability of the BxPC-3 cell line overexpressing *circATP13A1*

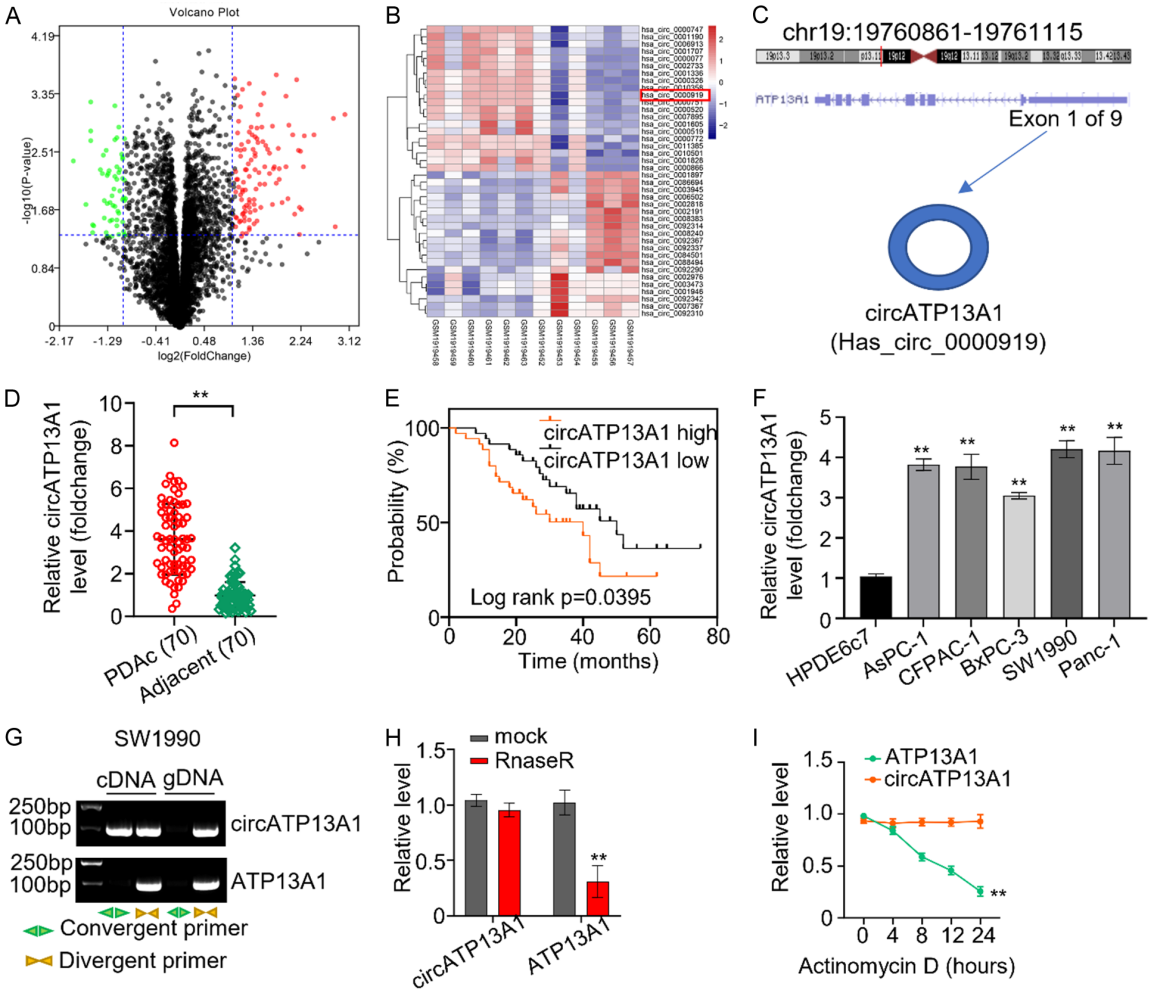

Figure 1. *CircATP13A1* is highly expressed in PDAC tissues and cell lines. A. The volcano plot shows the differential expression of circRNAs in PDAC tissues of cancer patients. B. The Limma R package reveals the differential expression of circRNAs in normal and tumor tissues. Circ-*ATP13A1* was significantly upregulated in PDAC cancer tissues relative to the adjacent normal tissues of 70 PDAC cancer patients downloaded from the GEO database. C. The schematic diagram displays the pre-mRNA structure of *ATP13A1*. D. QRT-PCR analysis indicates the significant upregulation of *circATP13A1* in PDAC tissues compared to adjacent normal tissues of PDAC. E. Seventy patients with PDAC were grouped based on *circATP13A1* expression levels (high vs low). High *circATP13A1* expression was generally associated with poor survival prognosis. F. Expression of *circATP13A1* in different PDAC cell lines, including HPDE6c7, AsPC-1, CFPAC-1, BxPC-3, SW1990, and Panc-1. G. Gel electrophoresis shows the amplification of *circATP13A1* and *ATP13A1 by* divergent and convergent primers in SW1990 cells. H. RNase R treatment effectively degrades linear *ATP13A1*, while RNase is ineffective in degrading *circATP13A1* in the SW1990 cell line. I. Actinomycin D significantly reduces the expression of linear *ATP13A1* in a time-dependent manner but cannot affect *circATP13A1* expression in the SW1990 cell line.

was significantly increased compared to the control ($P < 0.01$; **Figure 2B**). Moreover, the colony-forming ability was significantly reduced in the SW1990 cell lines transfected with the two siRNAs compared with si-NC. However, colony formation in the BxPC-3 cells was significantly increased when *circATP13A1* was overexpressed ($P < 0.01$; **Figure 2C**).

We assessed how the knockdown and overexpression of *circATP13A1* affected the invasion ability of the SW1990 and BxPC-3 cell lines. The result indicated that *circATP13A1* knockdown effectively reduced the invasion ability of SW1990 cells. However, the invasion ability of the BxPC-3 cells was significantly increased when *circATP13A1* was overexpressed ($P <$

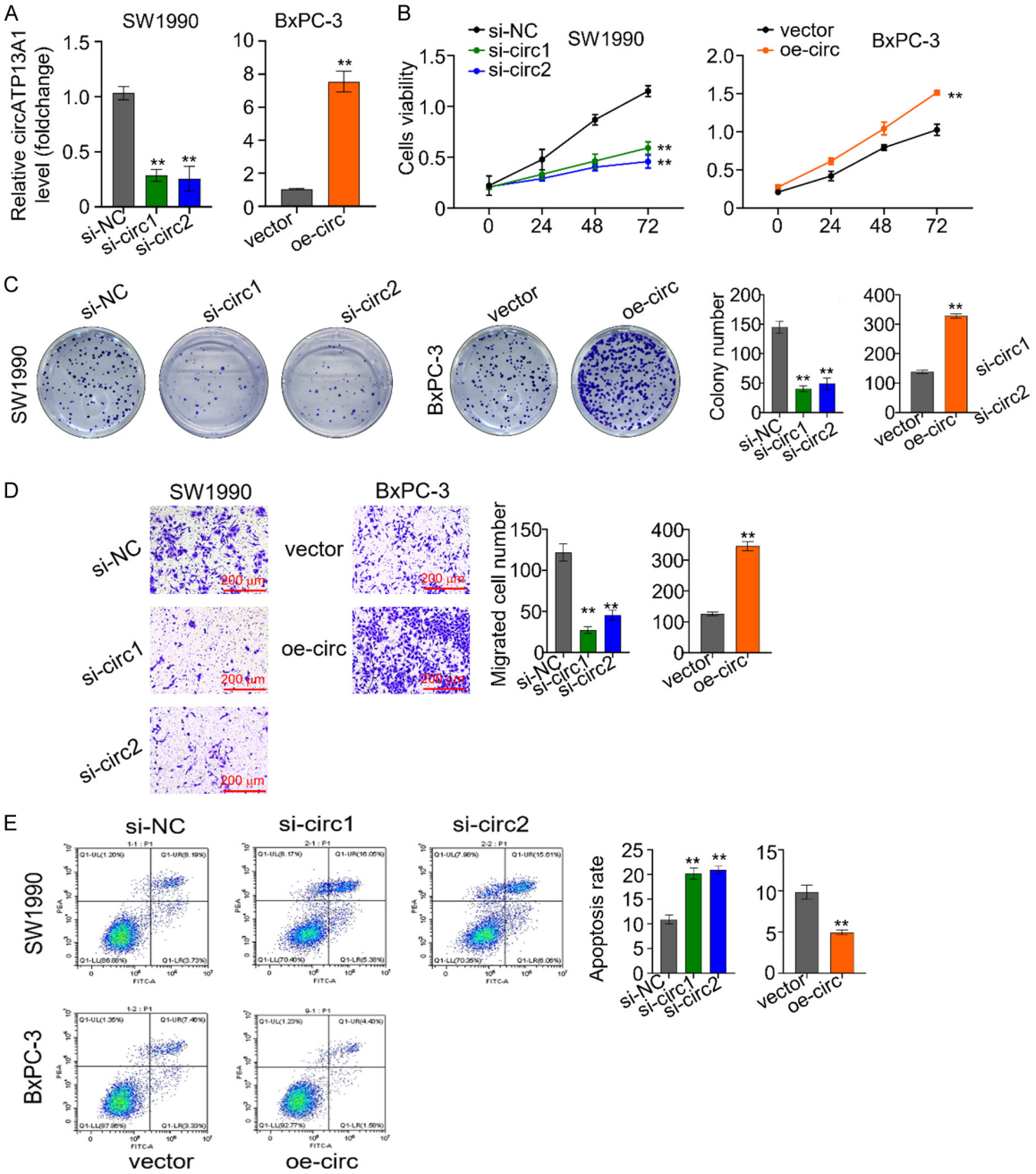

Figure 2. *CircATP13A1* promotes proliferation, metastasis, and anti-apoptosis of PDAC cell lines *in vitro*. A. QRT-PCR shows that si-circ1 and si-circ2 effectively knock down *circATP13A1* expression in the SW1990 cell line and oe-circ increases *circATP13A1* expression in the BxPC-3 cell line. B. Knockdown of *circATP13A1* by the two siRNAs (si-circ1 and si-circ2) significantly reduces cell viability in the SW1990 cell line compared with si-NC, and overexpressing *circATP13A1* significantly increases cell viability in the BxPC-3 cell line. C. Knockdown of *circATP13A1* by si-circ1 and si-circ2 reduces colony formation in SW1990, while overexpression *circATP13A1* by oe-circ significantly increases the colony-forming ability of PDAC. D. Knockdown of *circATP13A1* effectively reduces the invasion ability of SW1990 cells compared with si-NC, and the invasion ability of BxPC-3 cells was significantly increased. E. Flow cytometry reveals that cell apoptosis is significantly enhanced in SW1990 cell lines transfected with the two siRNAs, whereas cell apoptosis is significantly inhibited in BxPC-3 cells overexpressing *circATP13A1* (oe-circ).

0.01; **Figure 2D**). Furthermore, the flow cytometry revealed that cell apoptosis was significantly enhanced in the SW1990 cell lines transfected with the two siRNAs compared with the cells transfected with si-NC. In contrast, cell apoptosis was significantly suppressed in BxPC-3 cell lines overexpressing *circATP13A1* compared to control cells ($P < 0.01$; **Figure 2E**).

CircATP13A1 acts as a sponge for miR-186 and miR-326 in PDAC cell lines

Circular interactome predictions suggested that circ*ATP13A1* contained two binding sites for *miR-186* and *miR-326*. To verify the direct binding between circ*ATP13A1* and the two miRNAs, we conducted an RNA pull-down experiment to determine the enrichment of *miR-186* and *miR-326* by a biotin probe for circ*ATP13A1* in SW1990 and BxPC-3 cell lines. The results revealed that the circ*ATP13A1* probe effectively enriched *miR-186* and *miR-326* but the control probe did not ($P < 0.05$, **Figure 3A** and **3B**). We then performed a dual-luciferase reporter gene assay to further verify that circ*ATP13A1* targets *miR-186/miR-326*. We constructed wild-type circ*ATP13A1* (with targets for *miR-186* and *miR-326*, named "wt") and mutant circ*ATP13A1* ("mut1" denoting *miR-186* binding site mutation, "mut2" denoting *miR-326* binding site mutation, and "mut all" denoting mutations at both sites) (**Figure 3C**). The results revealed that the overexpression of *miR-186/miR-326* significantly decreased the luciferase activity of the cells transfected with the wt but had no effect on in the cells transfected with the "mut all" construct. In addition, the luciferase activity was moderately reduced in the cells transfected with either mut1 or mut2 ($P < 0.01$, **Figure 3D**). These results confirmed that circ*ATP13A1* directly binds to both *miR-186* and *miR-326*. We used qRT-PCR to assess the expression levels of *miR-186* and *miR-326* in SW1990 and BxPC-3 cell lines. The results indicated that *miR-186* and *miR-326* were upregulated when circ*ATP13A1* was knocked down in SW1990 cells. In contrast, the expression levels of *miR-186* and *miR-326* plummeted in BxPC-3 cells overexpressing circ*ATP13A1* ($P < 0.05$, **Figure 3E**). We also used qRT-PCR to analyze the expression of *miR-186* and *miR-326* in cancer and adjacent tissues from the 70 PDAC patients and found that *miR-186* and *miR-326* were significantly downregulated in PDAC cancer tissues compared to normal adjacent tissues ($P < 0.05$, **Figure 3F**).

HMGA2 is a common target of miR-186 and miR-326

We used the target scan to predict the gene targets of *miR-186* and *miR-326*. We found that both miRNAs could target the 3' UTR of *HMGA2* (**Figure 4A**). To confirm this prediction, we cloned the binding site sequences of *miR-186* and *miR-326*, *HMGA2* wild type (wt), and the mutated *HMGA2* sequences (mut1/mut2/mut all) into luciferase reporter genes. These reporter genes were co-transfected with miR-NC, *miR-186*, or *miR-326* mimics into SW1990 and BxPC-3 cells. The luciferase reporter assay indicated that luciferase activity in SW1990 and BxPC-3 cells transfected with wild type of *HMGA2*. In contrast, luciferase activity did not change in the cells containing mutated *HMGA2* ($P < 0.01$, **Figure 4B**). Further, we performed a RIP experiment to determine the enrichment of *miR-186*, *miR-326*, and *HMGA2* by anti-Ago2 and anti-IgG in SW1990 and BxPC-3 cell lines. qRT-PCR results showed that circ*ATP13A1*, *miR-186*, *miR-326*, and *HMGA2* were efficiently enriched on Ago2 compared to IgG ($P < 0.01$, **Figure 4C**). Furthermore, we examined the effect of *miR-186* and *miR-326* on *HMGA2* expression. qRT-PCR results revealed that *HMGA2* expression was significantly inhibited by *miR-186* and *miR-326* in SW1990 and BxPC-3 cell lines compared to the control ($P < 0.01$, **Figure 4D**). Western blot confirmed that *miR-186* and *miR-326* can inhibit the expression of HMGA2 in SW1990 and BxPC-3 cells (**Figure 4E**). Also, we assessed the expression of *HMGA2* in cancer and adjacent tissues from 70 PDAC patients. qRT-PCR results revealed that *HMGA2* expression level was higher in PDAC cancer tissues than in the normal adjacent tissue ($P < 0.01$, **Figure 4F**). Similarly, Western blot confirmed that HMGA2 was highly expressed in the PDAC cancer tissues compared to the normal adjacent tissues (**Figure 4G**).

CircATP13A1 promotes cell proliferation and metastasis via the miR-186/miR-326/HMGA2 axis

To identify the factors to which *CircATP13A1* interacts to promote PDAC progression, we employed qRT-PCR to assess the expression level of HMGA2. The results indicated that both si-circ+inh-*miR-186* and si-circ+inh-*miR-326* significantly reversed the downregulation of *HMGA2* by circ*ATP13A1* knockdown when compared with si-circ1, si-circ1+inh-NC, and normal control in the SW1990 cell line ($P < 0.01$; **Figure 5A**).

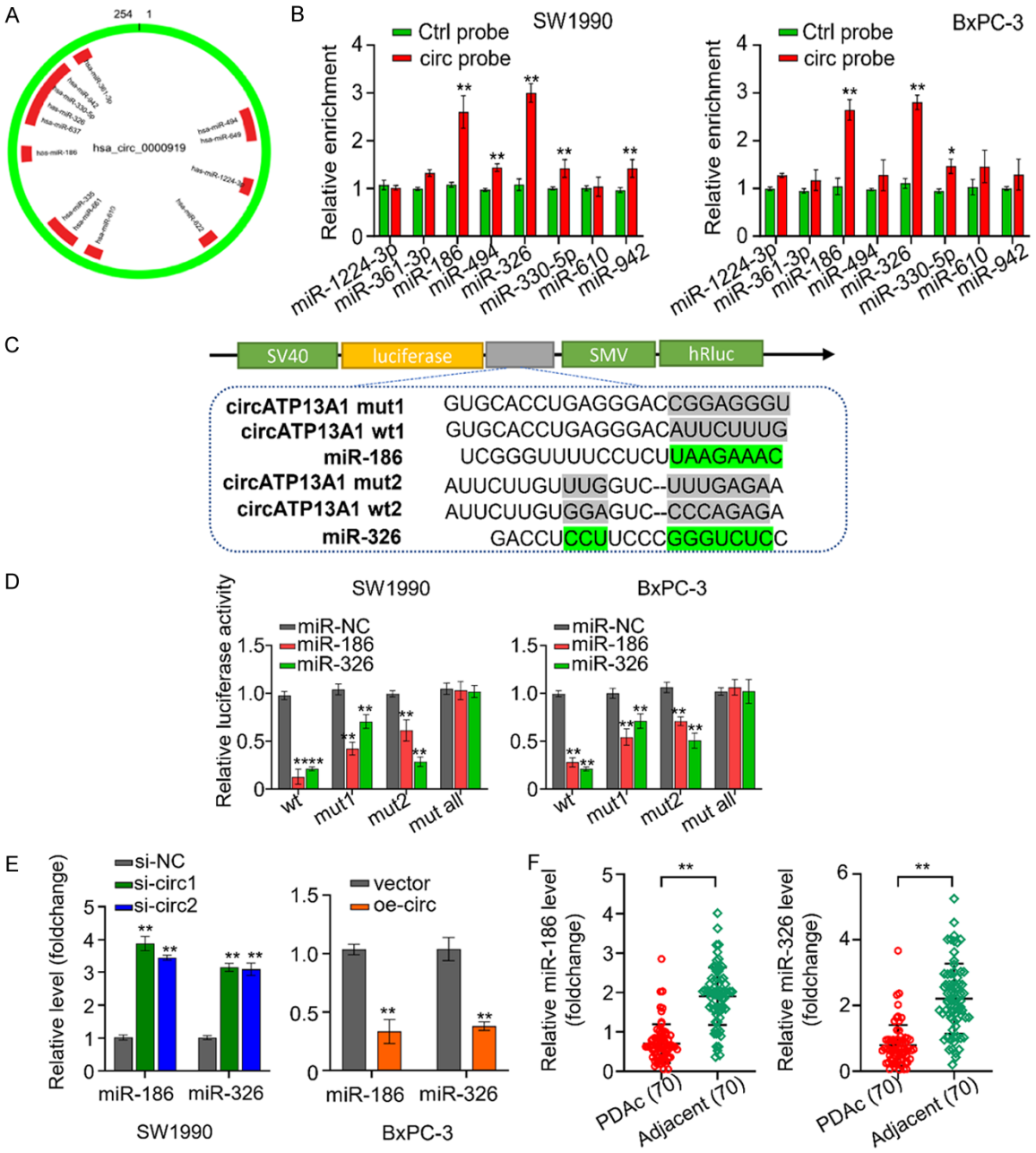

Figure 3. *CircATP13A1* sponges *miR-186* and *miR-326* in PDAC cell lines. A. Circular interactome analyses predicted that *circATP13A1* can target and bind to *miR-186* and *miR-326*. B. RNA pull-down experiments in SW1990 and BxPC-3 cell lines demonstrated that *circATP13A1* efficiently enriched *miR-186* and *miR-326* compared to other miRNAs and the control probe (ctrl). C. Constructed sequences of wild-type *circATP13A1*, mutant *circATP13A1*, *miR-186*, and *miR-326*. D. Luciferase reporter assay indicated a significant increase in the fluorescent intensity of the mutant *circATP13A1* sequence compared with the wild-type *circATP13A1* in the SW1990 and BxPC-3 cell lines. E. QRT-PCR showed that *miR-186* and *miR-326* were remarkably upregulated when *circATP13A1* was knocked down compared with the vector and normal control (Si-NC) in the SW1990 and BxPC-3 cell lines. F. QRT-PCR showed the expression of *miR-186* and *miR-326* in cancer and adjacent tissues of the 70 PDAC patients.

We used western blot to examine *HMGA2* expression levels in SW1990 cells with different treatments. Western blot showed that HMGA2 expression was significantly reduced by circ*ATP13A1* knockdown, which was recovered by the treatment of si-circ1+inh-*miR-186* or si-circ1+inh-*miR-326* (**Figure 5B**). Furthermore, we employed the CCK8 assay to examine

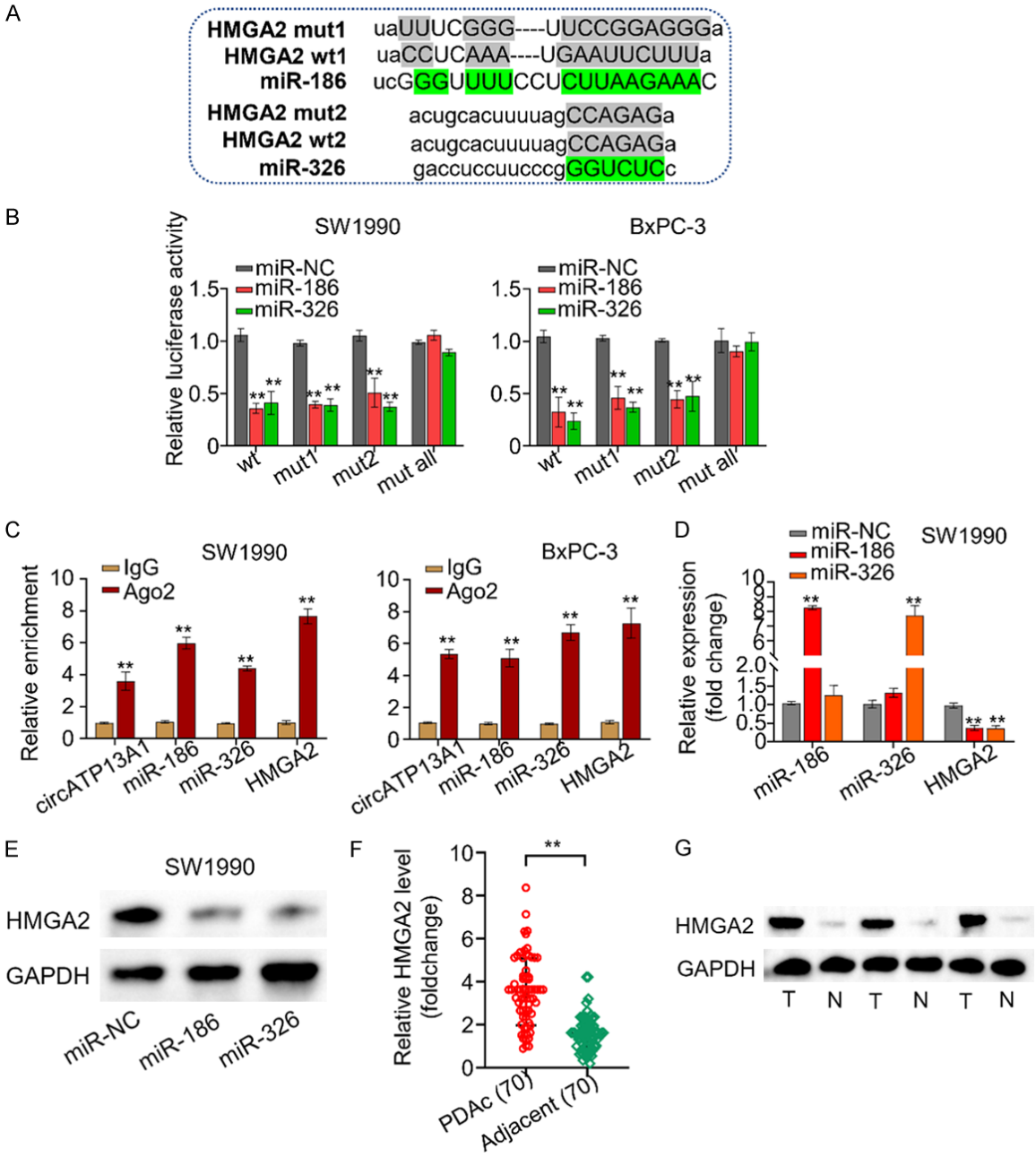

Figure 4. *HMGA2* is a common target of *MiR-186* and *MiR-326*. A. The construction of *miR-186*, *miR-326*, the wild-type *HMGA2* sequence, and the mutated *HMGA2* sequence. B. Luciferase activity in the wild-type *miR-186* and *miR-326* sequences was significantly reduced compared to miR-NC mimics in the SW1990 and BxPC-3 cell lines but did not change in the mutated *miR-186* and *miR-326* sequences compared with the wild-type *miR-186* and *miR-326* sequences in SW1990 and BxPC-3 cells. C. The RIP experiment shows that *circATP13A1*, *miR-186*, *miR-326*, and *HMGA2* were efficiently enriched on Ago2 compared to IgG. D. *HMGA2* expression was remarkably inhibited by *miR-186* and *miR-326* in SW1990. E. Western blot confirmed that *miR-186* and *miR-326* inhibited *HMGA2* expression. F. QRT-PCR showed that *HMGA2* expression was remarkably upregulated in PDAC cancer tissues compared to the normal adjacent tissue. G. Western blot confirmed that *HMGA2* was highly expressed in PDAC cancer tissues compared to normal adjacent tissues.

the cell viability of the SW1990 cells with various treatments (si-circ1, si-circ1+inh-NC, si-circ1+inh-*miR-186*, and si-circ1+inh-*miR-326*) at different time points (0 h, 24 h, 48 h, 72 h). The results indicated that the cell viability was significantly reduced in the si-circ1+inh-NC

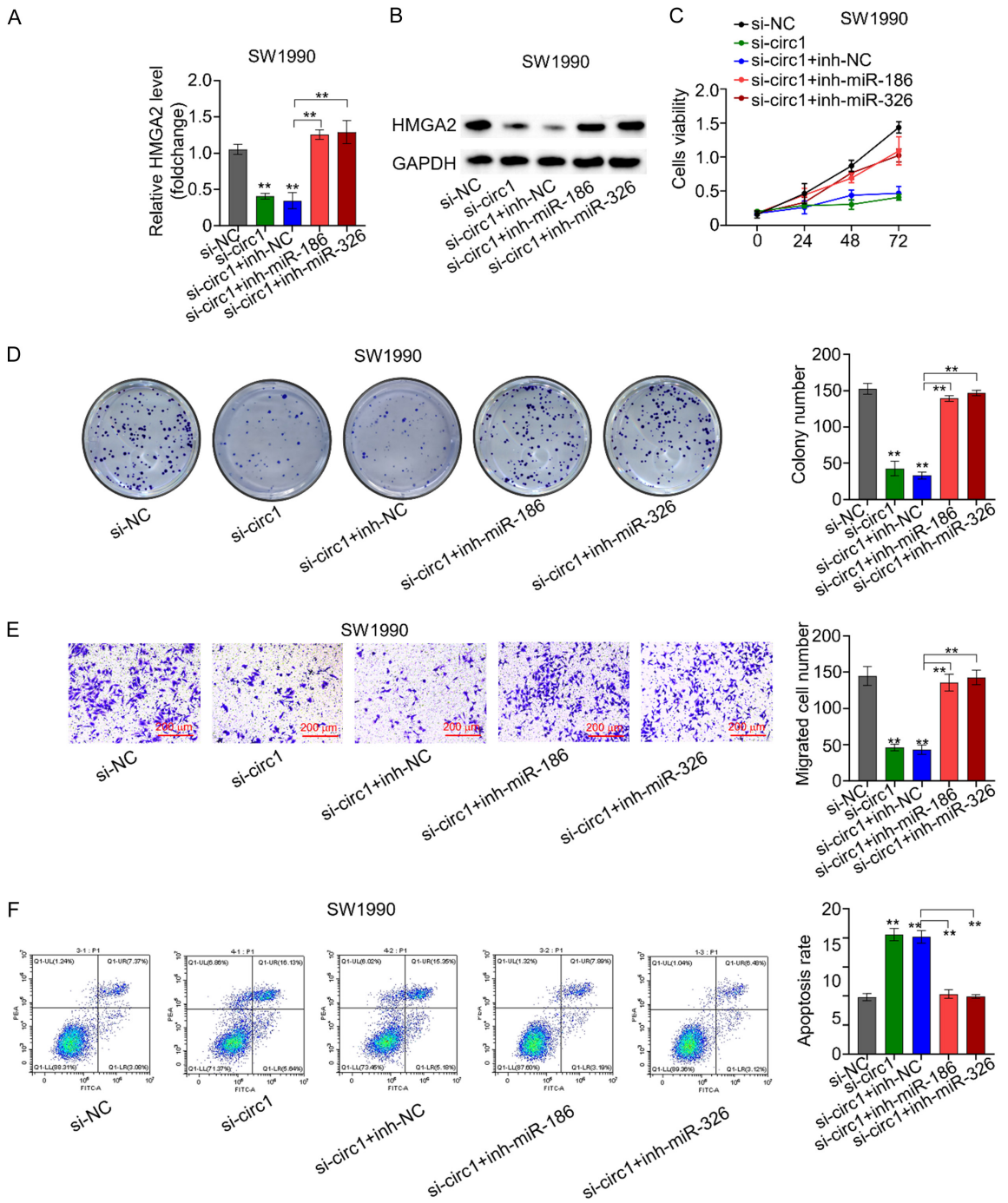

Figure 5. *CircATP13A1* promotes proliferation and metastasis via the *miR-186/miR-326/HMGA2* axis in PDAC cell lines. A. QRT-PCR analysis showed *HMGA2* expression levels in different groups. Both si-circ+inh-*miR-186* significantly reversed *HMGA2* downregulation resulting from *circATP13A1* knockdown in the SW1990 cell line. B. Western blot confirmed that *HMGA2* expression was significantly restored in the si-circ1+inh-*miR-186* and si-circ1+inh-*miR-326* groups with *circATP13A1* knockdown. C. CCK8 assay indicated that cell viability was significantly reduced in the si-circ1+si-circ1-inh-NC group compared with the normal control and other groups (si-circ1+si-circ1-inh-*miR-186*+si-circ1-inh-*miR-326*) in a time-dependent manner. D. A colony formation assay showed that the colony formation ability was significantly recovered when si-circ-inh-*miR-186* and si-circ-inh-*miR-326* were transfected in the SW1990 cell line. E. Transwell experiments revealed that si-circ-inh-*miR-186* and si-circ-inh-*miR-326* could restore the cell migration ability caused by *circATP13A1* in the SW1990 cell line. F. A flow cytometry experiment showed that the rate of apoptosis was remarkably higher in the si-circ and si-circ+inh-NC groups compared to other groups in SW1990 cell lines.

group compared with the control and other groups (si-circ1+inh-*miR-186* and si-circ1+inh-*miR-326*) ($P < 0.01$, **Figure 5C**). The colony formation assay was used to assess colony formation among different groups (si-circ, si-circ+inh-NC, si-circ+inh-*miR-186*, and si-circ+inh-*miR-326*). The colony formation ability was significantly recovered in SW1990 cells transfected with si-circ+inh-*miR-186* or si-circ+inh-*miR-326* compared to the control ($P < 0.01$, **Figure 5D**). Moreover, we performed the transwell experiment to detect the invasive ability of SW1990 cells transfected with si-NC, si-circ, si-circ+inh-NC, si-circ+inh-*miR-186*, or si-circ+inh-*miR-326*. The data showed that si-circ+inh-*miR-186* or si-circ+inh-*miR-326* could recover the reduced cell migration ability caused by *circATP13A1* knockdown compared to the si-circ and si-circ+inh-NC groups ($P < 0.01$, **Figure 5E**). Finally, we performed a flow cytometry analysis to determine the level of apoptosis of cells treated with si-NC, si-circ, si-circ+inh-NC, si-circ+inh-*miR-186*, or si-circ+inh-*miR-326*. The results revealed that cell apoptosis in the SW1990 cell line was significantly enhanced in the si-circ and si-circ+inh-NC groups compared to the other groups ($P < 0.01$; **Figure 5F**).

CircATP13A1 promotes PDAC tumor progression in vivo

To further assess the role of circ*ATP13A1* in PDAC progression, we conducted an *in vivo* tumor experiment using nude mice and stable PDAC cells transfected with circ*ATP13A1* knockdown. The results demonstrated that tumor growth was markedly inhibited in nude mice with circ*ATP13A1* knockdown compared to the control mice. Likewise, the tumor size in circ*ATP13A1* knockdown mice decreased significantly in a time-dependent manner compared to the control. The tumor weight in circ*ATP13A1* knockdown mice was also significantly reduced compared to the normal control ($P < 0.05$; **Figure 6A-C**). Finally, based on the results we showed above, we provided a schematic representation of the mechanism underlying the regulation of PDAC progression by circ*ATP13A1* (**Figure 6D**).

Discussion

Numerous studies have demonstrated the crucial role of circRNAs in various cancer types [28]. Here we, for the first time, found that circ*ATP13A1* was significantly upregulated in PDAC. Knockdown of circ*ATP13A1* inhibited cell proliferation, migration, and metastasis via the *miR-186/miR-326/HMGA2* axis, providing new insights into the regulation of cancer progression by circRNAs. CircRNA expression generally is tissue-specific and cancer-restricted [29]. Our study not only confirmed the significant upregulation of circ*ATP13A1* in PDAC but also correlated circ*ATP13A1* with poor survival rates of patients with PDAC. This finding is in line with the reports on the upregulation of other circRNAs in PDAC, such as circ*STX6* [30] and circ*BFAR* [31]. Overall, our results suggest that circ*ATP13A1* functions as an oncogene in PDAC and may hold potential as a prognostic biomarker for PDAC patients. CircRNAs have emerged as vital regulators in various cancers [32]. For example, circ_0007534 [12], circ_0030235 [33], and hsa_circ_0001649 [34] have been implicated in tumor cell proliferation and invasion as well as PDAC progression. In our study, we discovered that circ*ATP13A1* upregulation promoted PDAC cell proliferation, migration, invasion, and colony formation, while reducing apoptosis rates. On the other hand, circ*ATP13A1* knockdown significantly inhibited PDAC cell proliferation, colony formation, migration, and invasion, while increasing the apoptosis rate. These findings underscore the importance of circ*ATP13A1* in PDAC pathogenesis and suggest that targeting circ*ATP13A1* could be a promising therapeutic strategy for PDAC.

Numerous molecules including miRNAs have been identified as potential targets in research on cancers [35]. The fact that circRNAs contribute to cancer progression by sponging miRNAs has garnered attention [36, 37]. In our study, we found that *circATP13A1* sponged *miR-186* and *miR-326* in vitro, providing novel insights into the intricate mechanisms underlying PDAC progression. Notably, our results demonstrated that the expression of *miR-186* and *miR-326* was inversely correlated with circ*ATP13A1* expression levels. When circ*ATP13A1* expression was knocked down or overexpressed, *miR-186* and *miR-326* expression was upregulated or downregulated, respectively. This suggests that circ*ATP13A1* interacts with *miR-186* and *miR-326* to modulate PDAC progression.

To investigate the mechanism by which circ*ATP13A1* promotes PDAC progression, we first

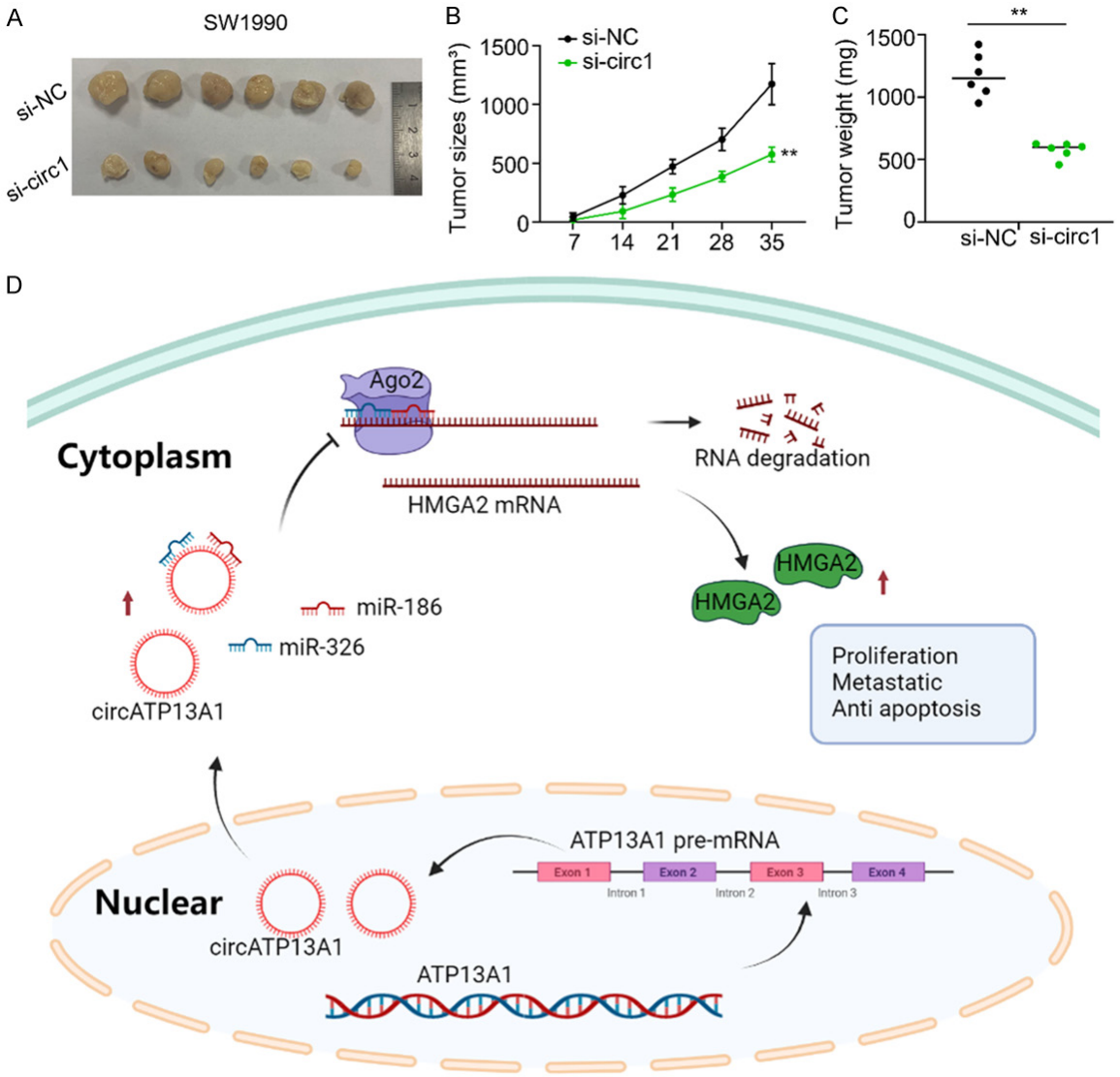

Figure 6. *CircATP13A1* promotes PDAC tumor progression *in vivo*. A. An *in vivo* experiment using nude mice revealed that the tumor size was significantly smaller in nude mice where *circATP13A1* was silenced compared to the control mice. B. The tumor size in *circATP13A1* knockdown mice was significantly reduced in a time-dependent manner compared to the control. C. Tumor weight in *circATP13A1* knockdown mice was significantly reduced compared to the normal control. D. The mechanism underlying the regulation of PDAC by *circATP13A1*.

confirmed that *HMGA2* was upregulated in PDAC cells. We also found that circ*ATP13A1* targets *HMGA2*. Two miRNAa, *miR-186* and *miR-326*, were remarkably downregulated by *HMGA2* overexpression. These findings align with studies reporting that *HMGA2* upregulation [38, 39] correlates with the progression of ovarian serous carcinoma and laryngeal squamous cell carcinoma. Our study, therefore, suggests that *HMGA2* is a potential target gene for *miR-186* and *miR-326* in PDAC cancer tissues. Moreover, we further explored the pathways by which circ*ATP13A1* promotes PDAC progression *in vitro*. Various pathways involved in PDAC progression have been identified, such as the Epithelial-Mesenchymal Transition (EMT) and the *miR-148a-3p/PD-L1* axis [40]. Our findings revealed that circ*ATP13A1* knockdown significantly reduced *HMGA2* expression, which was significantly restored by overexpressing *miR-186* and *miR-326*. Furthermore, our data indicated that the suppression of circ*ATP13A1* and *HMGA2* increased apoptosis rates while reducing cell proliferation, migration, and invasion in

PDAC, which were recovered by overexpressing *miR-186* and *miR-326*. These findings suggest that the *miR-186/miR-326/HMGA2* axis is the pathway through which circ*ATP13A1* promotes PDAC progression. *In vivo*, we observed a time-dependent decrease in tumor size and weight upon when circ*ATP13A1* expression was knocked down. This implies that circ*ATP13A1* contributes to tumor growth in PDAC patients. In future work, we will determine the expression levels of *miR-186, miR-326, HMGA2*, and *circATP13A1* in the tumors of si-NC and si-circATP13A1 mice to explore the clinical significance of *circATP13A1*.

In summary, our research provides compelling evidence that circ*ATP13A1* upregulation plays a crucial role in PDAC progression by promoting cell proliferation, viability, migration, and invasion in cancer patients. Our findings provide valuable insights into the molecular mechanisms underlying PDAC development and metastasis by elucidating the interactions between circ*ATP13A1*, *miR-186*, *miR-326*, and HMGA2. Furthermore, our study contributes to the growing body of knowledge on the diverse functions and regulatory roles of circRNAs in cancer biology. In addition, our work highlights the potential of circRNAs as diagnostic and prognostic biomarkers as well as therapeutic targets in PDAC and other cancer types.

Acknowledgements

Sponsored by Natural Science Foundation of Shanghai (18ZR1429100).

Written informed consent was obtained from all participants.

Disclosure of conflict of interest

None.

Address correspondence to: Drs. Xinyu Huang and Zhou Yuan, Department of Hepatobiliary and Pancreatic Surgery, Shanghai 6th People's Hospital Affiliated to Shanghai Jiao Tong University, School of Medicine, No. 600 Yishan Rd, Shanghai 200233, China. E-mail: h18930177490@21cn.com (XYH); zhouyuan851@163.com (ZY)

References

[1] Chen Q, Li J, Shen P, Yuan H, Yin J, Ge W, Wang W, Chen G, Yang T, Xiao B, Miao Y, Lu Z, Wu P and Jiang K. Biological functions, mechanisms, and clinical significance of circular RNA in pancreatic cancer: a promising rising star. Cell Biosci 2022; 12: 97.

[2] Rahib L, Smith BD, Aizenberg R, Rosenzweig AB, Fleshman JM and Matrisian LM. Projecting cancer incidence and deaths to 2030: the unexpected burden of thyroid, liver, and pancreas cancers in the United States. Cancer Res 2014; 74: 2913-2921.

[3] Sun X, Liu D, Ge N, Guo J, Wang S, Liu X, Wang G and Sun S. Recent advances in the potential use of circular RNA for the diagnosis and treatment of pancreatic cancer. Cancer Manag Res 2021; 13: 4251-4262.

[4] Long J, Luo GP, Xiao ZW, Liu ZQ, Guo M, Liu L, Liu C, Xu J, Gao YT, Zheng Y, Wu C, Ni QX, Li M and Yu X. Cancer statistics: current diagnosis and treatment of pancreatic cancer in Shanghai, China. Cancer Lett 2014; 346: 273-277.

[5] Saif MW. Pancreatic cancer: highlights from the 42nd annual meeting of the American Society of Clinical Oncology, 2006. JOP 2006; 7: 337-348.

[6] Zhang ZL, Bai ZH, Wang XB, Bai L, Miao F and Pei HH. miR-186 and 326 predict the prognosis of pancreatic ductal adenocarcinoma and affect the proliferation and migration of cancer cells. PLoS One 2015; 10: e0118814.

[7] Limb C, Liu DSK, Veno MT, Rees E, Krell J, Bagwan IN, Giovannetti E, Pandha H, Strobel O, Rockall TA and Frampton AE. The role of circular RNAs in pancreatic ductal adenocarcinoma and biliary-tract cancers. Cancers (Basel) 2020; 12: 3250.

[8] Rong Z, Xu J, Shi S, Tan Z, Meng Q, Hua J, Liu J, Zhang B, Wang W, Yu X and Liang C. Circular RNA in pancreatic cancer: a novel avenue for the roles of diagnosis and treatment. Theranostics 2021; 11: 2755-2769.

[9] Ma G, Li G, Fan W, Xu Y, Song S, Guo K and Liu Z. Circ-0005105 activates COL11A1 by targeting miR-20a-3p to promote pancreatic ductal adenocarcinoma progression. Cell Death Dis 2021; 12: 656.

[10] Zhang H, Ma X, Wang L, Li X, Feng D, Liu M, Li J, Cheng M, Song N, Yang X, Ba L, Lei Y, Zhang R, Zhu Y, Xu W and Qiao G. Circular RNA hsa_circ_0007367 promotes the progression of pancreatic ductal adenocarcinoma by sponging miR-6820-3p and upregulating YAP1 expression. Cell Death Dis 2022; 13: 736.

[11] Chen ZW, Hu JF, Wang ZW, Liao CY, Kang FP, Lin CF, Huang Y, Huang L, Tian YF and Chen S. Circular RNA circ-MTHFD1L induces HR repair to promote gemcitabine resistance via the miR-615-3p/RPN6 axis in pancreatic ductal adenocarcinoma. J Exp Clin Cancer Res 2022; 41: 153.

[12] Hao L, Rong W, Bai L, Cui H, Zhang S, Li Y, Chen D and Meng X. Upregulated circular RNA circ_0007534 indicates an unfavorable prognosis in pancreatic ductal adenocarcinoma and regulates cell proliferation, apoptosis, and invasion by sponging miR-625 and miR-892b. J Cell Biochem 2019; 120: 3780-3789.
[13] Galasso M, Sandhu SK and Volinia S. MicroRNA expression signatures in solid malignancies. Cancer J 2012; 18: 238-243.
[14] Iorio MV and Croce CM. MicroRNAs in cancer: small molecules with a huge impact. J Clin Oncol 2009; 27: 5848-5856.
[15] Li M, Marin-Muller C, Bharadwaj U, Chow KH, Yao Q and Chen C. MicroRNAs: control and loss of control in human physiology and disease. World J Surg 2009; 33: 667-684.
[16] Ren L and Yu Y. The role of miRNAs in the diagnosis, chemoresistance, and prognosis of pancreatic ductal adenocarcinoma. Ther Clin Risk Manag 2018; 14: 179-187.
[17] Liu Z, Zhang G, Yu W, Gao N and Peng J. miR-186 inhibits cell proliferation in multiple myeloma by repressing Jagged1. Biochem Biophys Res Commun 2016; 469: 692-697.
[18] Zhang TJ, Wang YX, Yang DQ, Yao DM, Yang L, Zhou JD, Deng ZQ, Wen XM, Guo H, Ma JC, Lin J and Qian J. Down-regulation of miR-186 correlates with poor survival in de novo acute myeloid leukemia. Clin Lab 2016; 62: 113-120.
[19] Zheng J, Li XD, Wang P, Liu XB, Xue YX, Hu Y, Li Z, Li ZQ, Wang ZH and Liu YH. CRNDE affects the malignant biological characteristics of human glioma stem cells by negatively regulating miR-186. Oncotarget 2015; 6: 25339-25355.
[20] Cai M, Wang Z, Zhang J, Zhou H, Jin L, Bai R and Weng Y. Adam17, a target of Mir-326, promotes Emt-induced cells invasion in lung adenocarcinoma. Cell Physiol Biochem 2015; 36: 1175-1185.
[21] Li D, Du X, Liu A and Li P. Suppression of nucleosome-binding protein 1 by miR-326 impedes cell proliferation and invasion in non-small cell lung cancer cells. Oncol Rep 2016; 35: 1117-1124.
[22] Wang Z, Sha HH and Li HJ. Functions and mechanisms of miR-186 in human cancer. Biomed Pharmacother 2019; 119: 109428.
[23] Mansoori B, Mohammadi A, Ditzel HJ, Duijf PHG, Khaze V, Gjerstorff MF and Baradaran B. HMGA2 as a critical regulator in cancer development. Genes (Basel) 2021; 12: 269.
[24] Mansoori B, Mohammadi A, Naghizadeh S, Gjerstorff M, Shanehbandi D, Shirjang S, Najafi S, Holmskov U, Khaze V, Duijf PHG and Baradaran B. miR-330 suppresses EMT and induces apoptosis by downregulating HMGA2 in human colorectal cancer. J Cell Physiol 2020; 235: 920-931.
[25] Chen X, Zeng K, Xu M, Liu X, Hu X, Xu T, He B, Pan Y, Sun H and Wang S. P53-induced miR-1249 inhibits tumor growth, metastasis, and angiogenesis by targeting VEGFA and HMGA2. Cell Death Dis 2019; 10: 131.
[26] Liu H, Li Q, Qi H, Du F and Qiu Y. Identification of circular RNA_0000919 as a potential diagnostic and prognostic biomarker of tongue squamous cell carcinoma using circular RNA microarray and reverse transcription-quantitative PCR analyses. Oncol Lett 2022; 24: 270.
[27] Yang T, Shen P, Chen Q, Wu P, Yuan H, Ge W, Meng L, Huang X, Fu Y, Zhang Y, Hu W, Miao Y, Lu Z and Jiang K. FUS-induced circRHOBTB3 facilitates cell proliferation via miR-600/NACC1 mediated autophagy response in pancreatic ductal adenocarcinoma. J Exp Clin Cancer Res 2021; 40: 261.
[28] Wu R, Tang S, Wang Q, Kong P and Liu F. Hsa_circ_0003602 contributes to the progression of colorectal cancer by mediating the miR-149-5p/SLC38A1 axis. Gut Liver 2023; 17: 267-279.
[29] Kristensen LS, Jakobsen T, Hager H and Kjems J. The emerging roles of circRNAs in cancer and oncology. Nat Rev Clin Oncol 2022; 19: 188-206.
[30] Meng L, Zhang Y, Wu P, Li D, Lu Y, Shen P, Yang T, Shi G, Chen Q, Yuan H, Ge W, Miao Y, Tu M and Jiang K. CircSTX6 promotes pancreatic ductal adenocarcinoma progression by sponging miR-449b-5p and interacting with CUL2. Mol Cancer 2022; 21: 121.
[31] Guo X, Zhou Q, Su D, Luo Y, Fu Z, Huang L, Li Z, Jiang D, Kong Y, Li Z, Chen R and Chen C. Circular RNA circBFAR promotes the progression of pancreatic ductal adenocarcinoma via the miR-34b-5p/MET/Akt axis. Mol Cancer 2020; 19: 83.
[32] Ng WL, Mohd Mohidin TB and Shukla K. Functional role of circular RNAs in cancer development and progression. RNA Biol 2018; 15: 995-1005.
[33] Xu Y, Yao Y, Gao P and Cui Y. Upregulated circular RNA circ_0030235 predicts unfavorable prognosis in pancreatic ductal adenocarcinoma and facilitates cell progression by sponging miR-1253 and miR-1294. Biochem Biophys Res Commun 2019; 509: 138-142.
[34] Jiang Y, Wang T, Yan L and Qu L. A novel prognostic biomarker for pancreatic ductal adenocarcinoma: hsa_circ_0001649. Gene 2018; 675: 88-93.
[35] Fu Z, Wang L, Li S, Chen F, Au-Yeung KK and Shi C. MicroRNA as an important target for anticancer drug development. Front Pharmacol 2021; 12: 736323.
[36] Bizzarri AR and Cannistraro S. Direct interaction of miRNA and circRNA with the oncosup-

pressor p53: an intriguing perspective in cancer research. Cancers (Basel) 2021; 13: 6108.
[37] Xiang Y, Tian Q, Guan L and Niu SS. The dual role of miR-186 in cancers: oncomir battling with tumor suppressor miRNA. Front Oncol 2020; 10: 233.
[38] Hetland TE, Holth A, Kaern J, Florenes VA, Trope CG and Davidson B. HMGA2 protein expression in ovarian serous carcinoma effusions, primary tumors, and solid metastases. Virchows Arch 2012; 460: 505-513.
[39] Ma LJ, Wu J, Zhou E, Yin J and Xiao XP. Molecular mechanism of targeted inhibition of HMGA2 via miRNAlet-7a in proliferation and metastasis of laryngeal squamous cell carcinoma. Biosci Rep 2020; 40: BSR20193788.
[40] Fu X, Sun G, Tu S, Fang K, Xiong Y, Tu Y, Zha M, Xiao T and Xiao W. Hsa_circ_0046523 mediates an immunosuppressive tumor microenvironment by regulating MiR-148a-3p/PD-L1 axis in pancreatic cancer. Front Oncol 2022; 12: 877376.